Limited-view ultrasonic guided wave tomography using an adaptive regularization method

Rao, Jing; Ratassepp, Madis; Fan, Zheng

2016

Rao, J., Ratassepp, M., & Fan, Z. (2016). Limited-view ultrasonic guided wave tomography using an adaptive regularization method. Journal of Applied Physics, 120(19), 194902-.

https://hdl.handle.net/10356/83622

https://doi.org/10.1063/1.4967790

Limited-view ultrasonic guided wave tomography using an adaptive regularization method

Jing Rao, Madis Ratassepp, and Zheng Fan[a)]
School of Mechanical and Aerospace Engineering, Nanyang Technological University, 50 Nanyang Avenue, Singapore 639798, Singapore

(Received 14 August 2016; accepted 1 November 2016; published online 15 November 2016)

Ultrasonic guided waves are useful to assess the integrity of a structure from a remote location. Recently, tomography techniques have been developed to quantitatively estimate the thickness map of plate-like structures based on the dispersion characteristics of guided waves. In many applications only limited locations are available to place transducers. The missing viewing angles lead to artifacts which can degrade the image quality. To address this problem, this paper applies the regularization method to synthesize the missing components. The regularization technique is performed by an adaptive threshold approach to the limited view reconstruction. The effectiveness of this method combined with the full waveform inversion method is demonstrated by using numerical simulations as well as experiments on an irregularly shaped defect and two flat-bottom defects. The results indicate that the additional components obtained from the regularization method can significantly reduce the artifacts, leading to better reconstruction accuracy. *Published by AIP Publishing.* [http://dx.doi.org/10.1063/1.4967790]

I. INTRODUCTION

Guided wave tomography (GWT) is an attractive method to measure the thickness map of large structures quantitatively without requesting direct access to the interested area. It is based on the dispersion relations of particular guided modes, and the reconstructed velocity maps of guided waves are converted to thickness maps.[1–3] An ideal reconstruction can be obtained when the measurement is conducted from as many angles around the inspection area as possible—a full view configuration. However, only a limited number of angles are available in reality. For example, the assessment of pipelines using GWT is usually carried out by two transducer rings on each side of the inspection area, thus, limiting the viewing angles. Reconstruction from incomplete data is ill-posed, which suggests that more than one solution can fit the measured data.[4] The missing angles will typically result in noticeable artifacts, which degrade the quality of reconstruction by varying reconstructed velocities and generating ghost features.[5] Such problems also widely exist in other related areas, such as x-ray tomography,[6] seismology,[7] and medical ultrasound applications.[8] Efforts have been made to improve the reconstruction from the limited view, which can be broadly divided into three groups, including statistical, probabilistic algorithms,[9] minimization[10,11] and projection regularization methods.[5,12]

Two typical approaches of statistical, probabilistic algorithms are maximum entropy techniques[13] and Bayesian methods.[14] These two approaches allow the incorporation of the prior information about the maximum entropy and the general shape or structure of the object, respectively. When the prior information is restrictive enough, good estimations of the unknown components can be obtained, thereby reducing the image artifacts. The main challenge of these algorithms is the high computational complexity and the sensitivity to errors in the data.[15]

The minimization method is to obtain a solution that can best fit to the measured data and also match a particular constraint. Weighting variables are used to achieve the balance between the measured data and the constraint. At each iteration in the inverse model, the residual data (difference between computed results and the measured data) is minimized. Ultimately, they will converge to a single fitting minimum. This method is widely used for the total variation minimization and also combined with regularization.[10,11] However, the performance of minimization algorithms is largely dependent on the choice of appropriate constraints, which are complex to choose. Moreover, these methods are also computationally expensive.[16]

The projection regularization method can be used in combination with direct imaging approaches in the reconstructions. This projection process indicates that in each step a regularization restriction can be carried out by directly applying particular constraints to the image. Positivity is a common example of this method.[12] It enforces the constraint of positivity on each pixel of the estimated image and penalizes negative values to be zero. Huthwaite[5] introduced a projection-based regularization approach of Virtual Image Space Component Iterative Technique, which combined the image regularization approach with a linearized forward solver to determine the unknown components. Compared with a static regularization like positivity, better values of the unknown components can be obtained by iteratively using the thresholding to the reconstruction. This approach overcomes the limitation of complex implementation and intensive computation in the statistical, probabilistic algorithms. Compared with the minimization algorithms which work on the continuous functions to match the measured

[a)]Electronic mail: ZFAN@ntu.edu.sg

data with the restriction, the restriction of the projection regularization method does not rely on continuous defining of matching degree with the image.

Recently, a nonlinear inverse scattering model has been developed for GWT.[17] It uses a numerical solver to predict the waveform of signals propagating through the inspection area, and an iterative inverse model to reconstruct the thickness map based on the dispersion relations. This full waveform inversion (FWI) method uses a nonlinear data fitting procedure which allows higher order scattering from the defects to be considered.[18] This paper combines the FWI method with the adjustable thresholding regularization method to address the challenges in the limited view GWT. In this study, the fundamental anti-symmetric Lamb wave mode (A_0) was employed for defect identification, which has been demonstrated as a sensitive mode to thickness variations around certain frequency.[19]

The paper is organized as follows. In Section II, after a brief overview of the challenges in the limited view problem, the theory of the FWI with adaptive thresholding regularization is introduced. This method is validated by both Finite Element (FE) simulations and experiments. The setup is introduced in Section III and the reconstructions of an irregularly shaped defect, as well as two defects are shown in Section IV. In Section V, discussions are carried out to explore the effect of the length of the array to the reconstructed image. Conclusions are summarized in Section VI.

II. THEORY

A. Analysis of the limited view problem

For simplicity, the limited view problem is analyzed in the framework of a Born model with the far field assumption. Under these assumptions, the scattered field U_s can be described by the following equation:[20,21]

$$U_s \approx -\int_{\Omega} e^{ik(\hat{s}_0-\hat{s})x} O(x)dx, \tag{1}$$

where Ω represents the domain of the scatterer and k is the wavenumber. $\hat{s}_0$ and $\hat{s}$ are the directions of the incident illumination and the reception, respectively. $O(x)$ is the object function, which is the mathematical representation of the scatterer. The scattered field can be effectively given by a Fourier transform of the object function $\tilde{O}$ in the spatial frequency domain

$$U_s(\hat{s}_0, \hat{s}) \approx -\tilde{O}[k(\hat{s}_0 - \hat{s})]. \tag{2}$$

It means that the signal obtained from each source-receiver corresponds to the Fourier component of the object function at $k(\hat{s}_0 - \hat{s})$. As shown in Figs. 1(a) and 1(b), the ideal reconstruction of the object can be obtained by using the information from all possible illumination and reception angles for all frequencies within a disk.[20] The effect of the limited view is to leave sections, where the estimation of the Fourier transform of the object cannot be obtained. This introduces a low pass filter for the areas, where there is no data. Typical limited view problem with a pair of parallel linear arrays

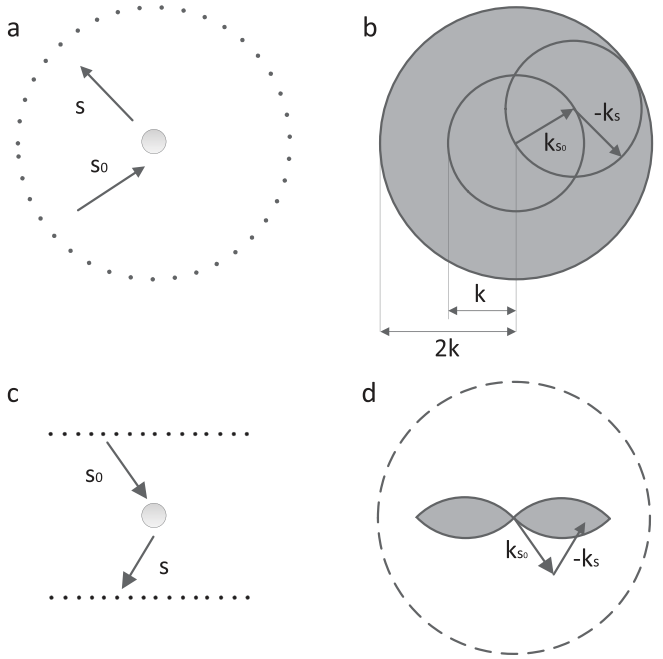

FIG. 1. 2D Fourier transform based on the Born approximation. The full view array (a); the corresponding Fourier components obtained from each layout (b); a pair of parallel linear arrays with a source array above the defect and a receiver array below it (c); and the corresponding Fourier components (d).

measuring the transmission data and its filtered wavenumber spectrum are shown in Figs. 1(c) and 1(d). More detailed discussions can be found in References 7 and 21.

Therefore, the key issue in the limited view reconstruction is to have a good estimation of the missing components, and this could be obtained from the prior information. For example, the reconstructed values of the scatterer should be equal or larger than the background value.[22]

B. Regularization to synthesize unknown components

In order to reduce the artifacts caused by the limited view, the regularization approach based on a prior information via the iterative algorithm is applied to obtain more suitable data for the unknown components. An example of this process used in References 5 and 22 is illustrated in Fig. 2. The regularization assumption is made that the values of the scatterer are the same or larger than the background. Based on the far field assumption, the known Fourier components can be directly obtained from the data, as shown in Fig. 2(a), which is similar as Fig. 1(d). The values outside the known components are zero. The image shown in Fig. 2(b) can be obtained directly from the Fourier components shown in Fig. 2(a) by taking inverse Fourier transform. Since unknown components are set to zero, the reconstruction will become a low-pass filtered version of the true image. This will result in "x" shaped artifacts.[7] Then, the reconstruction is regularized by setting the negative values to the background value of zero and the forward Fourier transform of this image is taken, as illustrated in Figs. 2(c) and 2(d), respectively. It can be seen that the unknown components that are zero in the wavenumber space image become now non-zero values,

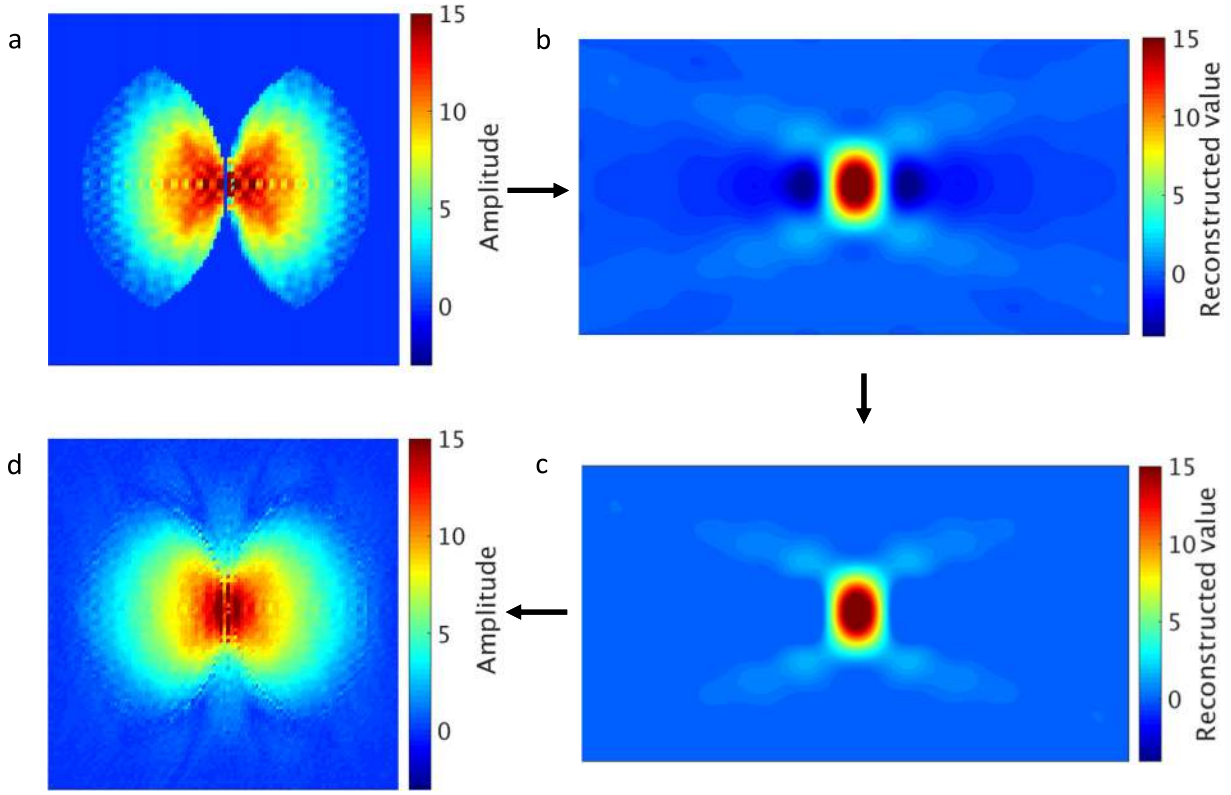

FIG. 2. Applying the approach used by Sung *et al.*[22] to synthesis unknown Fourier components by regularization. Fourier components from a limited view (a), the reconstruction obtained by using Fourier transforming (b), then the regularization is applied in (c), and the additional information can be obtained by regularization (d).

which suggest that additional information from the missing components is obtained.

C. Adaptive thresholding regularization method

In many cases, although the artifacts linked with the limited-view problem mask the lower amplitude features, the peak features are relatively well reconstructed,[7] as demonstrated in Fig. 3(a). This characteristic can be exploited by an adaptive thresholding approach.[5] In this method, a threshold is applied to the image, which is below the artifacts level but above the level of peak feature, as shown in Fig. 3(b). Below this threshold level, all values are maintained and values above this threshold are set to the background. Such process can be used to populate the unmeasurable components due to the limited view. The extra information from the missing angles obtained by using this regularization is combined with the measured data, and thus, the artifacts above this threshold will be reduced, as shown in 3(c). As the artifacts reduce at later iterations, the threshold level can be gradually increased towards the background level until most of the artifacts are removed.

It should be noted that this threshold method can be used in either case of the reconstructed value above or below the background. The threshold can be defined as[5]

$$\mathrm{m}_{reg}(x) = \begin{cases} \mathrm{m}(x) & if \dfrac{|\mathrm{m}(x) - \mathrm{m}_0|}{\max|\mathrm{m}(x) - \mathrm{m}_0|} < l_e \\ \mathrm{m}_0 & \text{otherwise,} \end{cases} \tag{3}$$

where $\mathrm{m}(x)$ is the model parameter at x, m_0 being the level of the background, and l_e is the threshold fraction.

D. Implementation of the regularization method in guided wave tomography

In this paper, the FWI algorithm is used as the reconstruction algorithm for GWT, which has been introduced in details previously.[17] It uses a forward model to predict the scattering measurements in a 2D acoustic model and an inverse model to update the velocity map iteratively, which is then associated with the thickness map via the dispersion curves. This method allows phase distortion through the scatterer and higher order scattering effects to be considered in its numerical solver; thus, it provides good accuracy of the reconstruction.

Fig. 4 outlines the flowchart of the regularization method in combination with the FWI algorithm. Initially, the unmeasurable components are set to zero. The image is obtained by using the measured, limited view data based on the FWI algorithm. Then the regularization based on the adaptive thresholding method is applied. At each threshold level, a non-linear forward solver of the current regularized image is used to generate unknown data in the FWI algorithm, then the inversion is followed to perform a reconstruction from that. The information included in the unknown components contributes to the improvement in the image caused by the regularization. Thus, the solution incorporates this additional information into the measured, limited-view

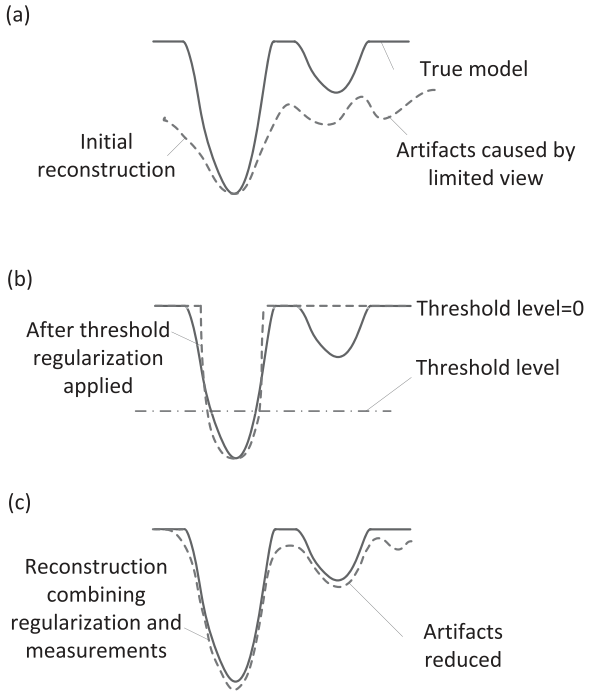

FIG. 3. 1D example illustrating the schematic outline of the method of the thresholding regularization. The standard limited view reconstruction (a), a threshold used in the image (b) and the next regularized reconstruction (c).

data, which can achieve a better estimation of the image for the next iteration. This process is repeated until the convergence is achieved. The mean square error (MSE) can be used as a criterion of convergence, similarly as in References 5 and 23

$$MSE_{(FWI)} = \sqrt{\frac{\sum_{pi=1}^{N_{pi}} \left(T_{pi}^{(i)} - T_{pi}\right)^2}{\sum_{pi=1}^{N_{pi}} T_{pi}^2}}, \quad (4)$$

where T_{pi} is the original thickness at pixel pi, $T_{pi}^{(i)}$ is the reconstruction of the thickness at pixel pi for the ith iteration, and N_{pi} represents all pixel number in the reconstructed image. The value of MSE is decreasing with the increasing of the number of the iteration, and then it can converge to a single value. Experience showed that the convergence for a single frequency can be achieved in 10 to 20 iterations.

It is important to set an appropriate threshold fraction in the regularization, and in this paper, it can be expressed as $f^{(n+1)} = p(f^{(n)} + q) - q$, similar to the literature.[5] The parameter p is used to define the degree of threshold increase at each iteration and q is the asymptotic limit. In this paper, $p = 0.8$, $q = 0.2$, and $f^{(0)} = -0.6$ were used. The background level is set to zero, and so the threshold fraction below this level is negative. The initial value $f^{(0)}$ can be adjusted according to the particular case. The standard limited view FWI algorithm was firstly carried out by using multiple frequencies.[17] Based on the obtained results from the final frequency, we chose to perform each regularization iteration for several FWI iterations. In this paper, after one regularization iteration,

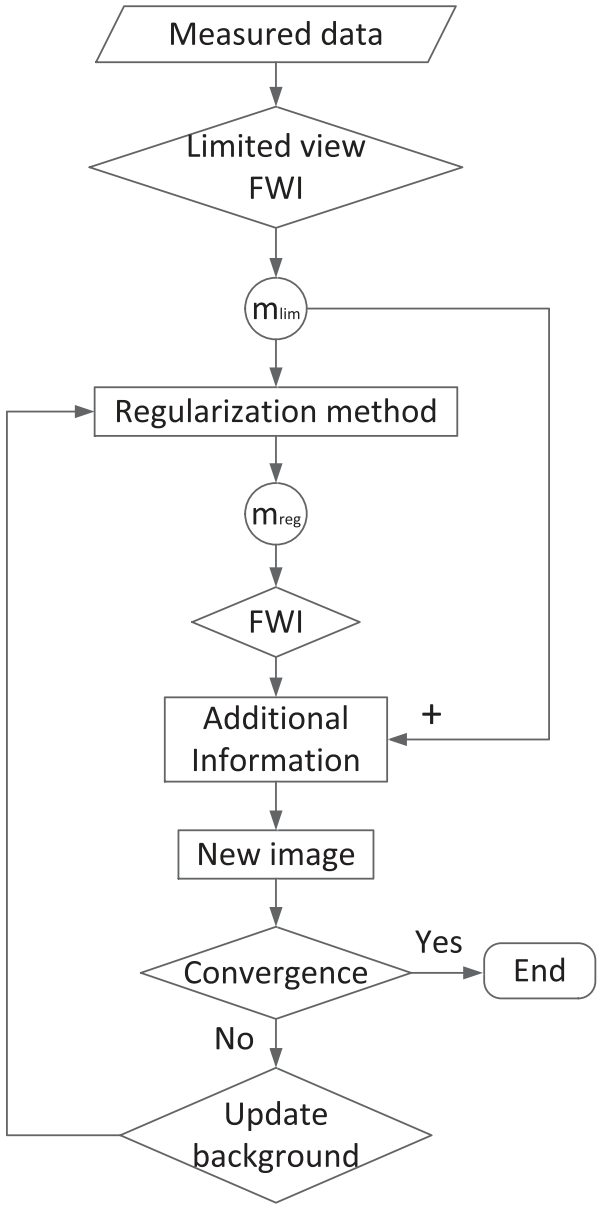

FIG. 4. The flowchart of regularization with the FWI algorithm for a limited view configuration.

around 10 FWI iterations are performed to update the background. This process is iterated through repeating application of the regularization until convergence.

III. VALIDATION METHODS

A. Problems studied

In this study, two types of defects: irregularly shaped defect and axisymmetric flat-bottom circular ones, are considered on an aluminum plate (Young's modulus = 70.8 GPa, Poisson's ratio = 0.33 and density = 2700 kg/m^3) with the dimension of 1100 mm × 1100 mm × 10 mm. The irregularly shaped defect has the largest size of around 100 mm, with depth of 3 mm. The flat-bottom defect can be described by the surface diameter, the bottom diameter, and the defect depth.[24] In the case of two flat-bottom defects, each defect is offset by 40 mm from the center of the plate, in the horizontal direction.

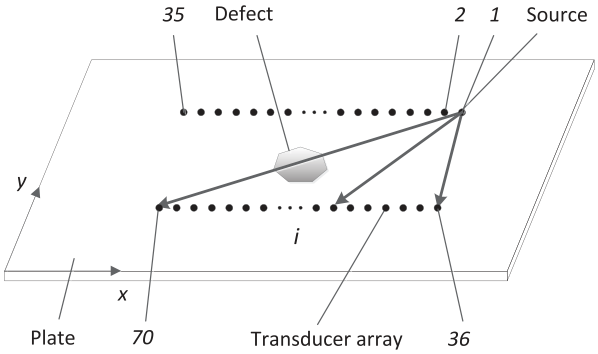

FIG. 5. The configuration of a pair of parallel linear transducer arrays for guided wave tomography on a plate.

The larger defect has the surface diameter of 60 mm, the bottom diameter of 44 mm, and the depth of 50% of the nominal plate thickness. The smaller defect has the surface and bottom diameters of 42 mm and 34 mm and its thickness reduction is 20%.

B. Numerical modeling

To validate the proposed algorithm, 3D FE simulations were performed for the above two cases. The cubic-shaped brick elements were used to model the plate, with the element size of 1 mm. The thickness variation of defects can be modeled by removing the elements from the mesh. Absorbing layers were applied to minimize reflections from the edges.[25] A pair of parallel linear transducer arrays were modeled, as shown in Fig. 5. A 5 cycle Hanning-windowed tone-burst signal at 50 kHz was simulated as the input signal. For a given excitation point in one array, the A_0 mode was generated by applying an out-of-plane force and the wavefields were measured by all receivers in the other array. The setup of the arrays is slightly different in the two cases. For the irregularly shaped defects, each array consists of 35 different generator/monitor positions equally separated by 20 mm ($\simeq$0.6 wavelengths at 60 kHz), and the space between two parallel linear transducer arrays is 150 mm. For the cases of two defects, each array has 17 generator/monitor positions separated by 40 ($\simeq$1.2 wavelengths at 60 kHz) and the space between the two arrays is 200 mm.

C. Experimental procedures

The experimental setup is shown in Fig. 6, with the defects introduced by a computer numerical control (CNC) milling machine in the same dimension as in FE simulations. The A_0 mode was excited by the PZT transducer (Panametrics V1011) at one position, which was coupled to the plate through a small area by an aluminum disk with the diameter of 10 mm and the thickness of 0.5 mm.[26] The displacement normal to the surface was measured by a Polytec OFV-505 laser vibrometer. In the measurement, a 5 cycle Hanning-windowed tone-burst signal centred at 50 kHz was generated by a Tiepie Handyscope HS3.

To avoid reflections from the plate edges, only transmitted signals were measured, and thus, the measurements were performed along a one linear transducer array, as shown in Fig. 6. By repeating this process, a matrix of 70×35 signals obtained from the irregularly shaped defect and a 34×17 matrix of all source-receiver combinations based on two flat-bottom defects can be generated from two measurements. The unwanted parts from the measured signals can be removed by using a gating function.[2] Before using these signals in the inversion, the calibration of obtained signals was conducted in the similar way as in the previous work.[17]

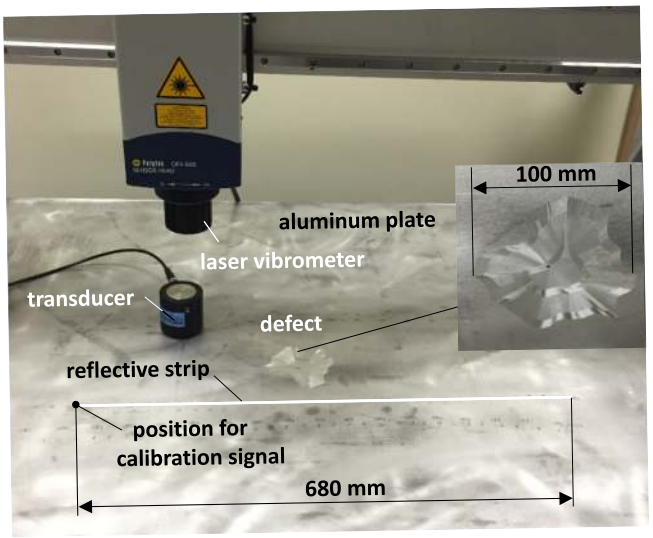

FIG. 6. The experimental setup on an irregularly shaped defect.

IV. RESULTS AND ANALYSIS

A. Irregularly shaped defect

Fig. 7(a) presents the original model of an irregularly shaped defect, as in the experiment, by using a pair of parallel linear transducer arrays. Each array has 35 transducers separated by 20 mm. The defect has a complex shape and smooth variations in the thickness. The largest size of this defect is about 100 mm and its depth is 3 mm. Three sequential frequencies of 35, 46, and 60 kHz were used in the standard limited view FWI algorithm, with 40 iterations per frequency. Then, based on the results obtained from 60 kHz, the regularization is applied and 10 FWI iterations are used to update the background. As the artifacts decrease with increasing number of iterations, the level of the threshold can be slightly increased. This process is repeated until it converges. The work was run on a HP Z820 work station with 32-core and 128 G memory. The total process took around 2 h to generate regularized results shown in Fig. 7(c).

It can be seen from Fig. 7(b) that the standard FWI limited view reconstruction based on the FE simulation has slight elongation in the shape of the defect and clear "x" shaped artifacts. Compared to the full view configuration, the relatively small range of viewing angles can slightly distort the defect. However, the quality of the resolvable area is not degraded in general. These diagonal artifacts are common results in a limited view configuration.[27] The reason is that the unknown components are set to zero in the standard limited view reconstruction; thus, the limited view reconstruction will lead to a filtered version of the true image and

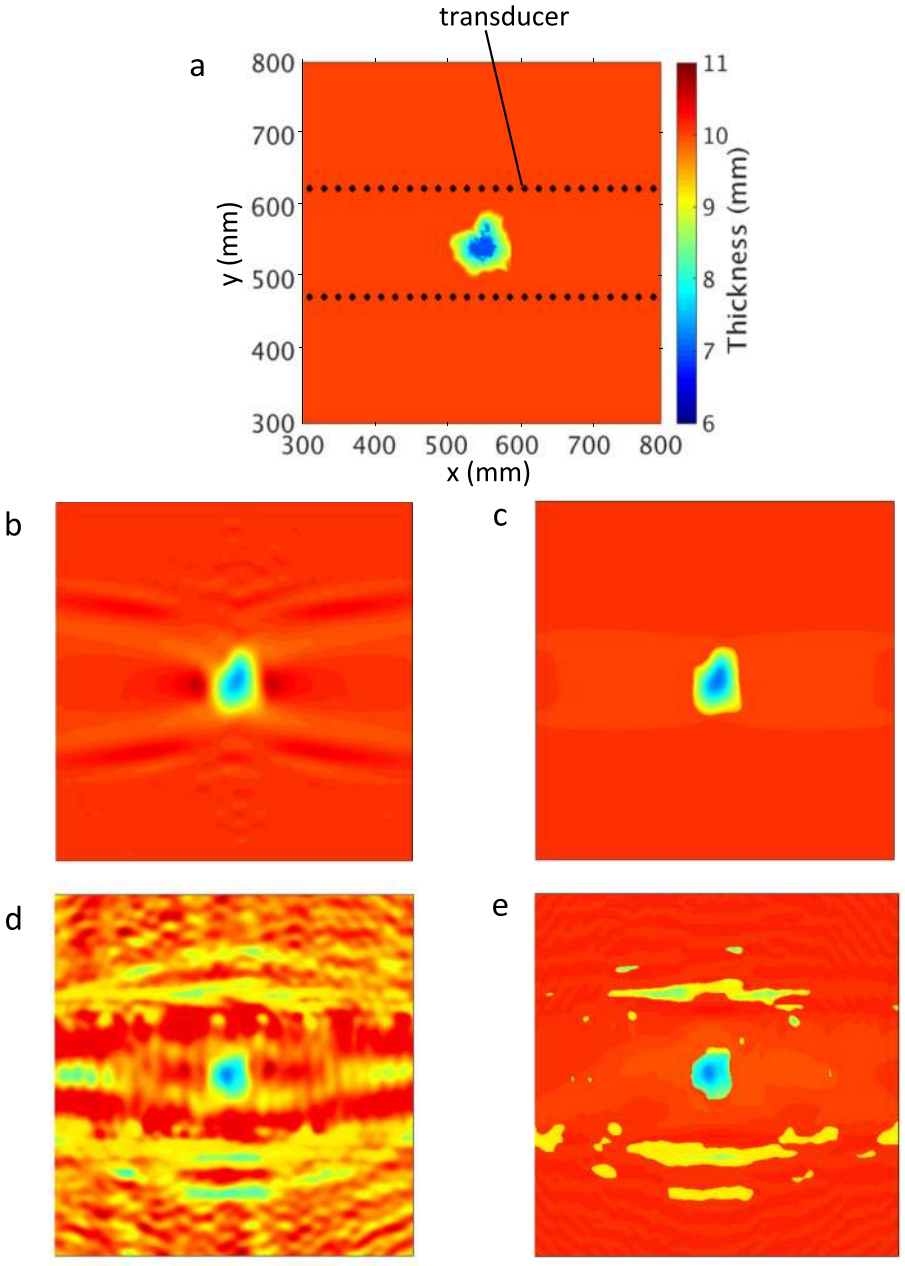

FIG. 7. Reconstructions with an irregularly shaped defect by a pair of parallel linear transducer arrays. Original model (a), the standard FWI limited view reconstruction (b), and the regularized reconstruction (c) based on the FE model; the standard limited view reconstruction (d), and the regularized reconstruction (e) in the experiment. (b)–(e) follow the same color bar and scale in the axes as in (a).

this filtering will cause artifacts in the reconstruction. Some artifacts observed at locations of two arrays are mainly caused by the undersampling of the wavefield as the separation of the transducer locations is below the Nyquist requirement of half wavelength.[17] Fig. 7(c) shows the image after regularization which slightly improves the defect representation, and more importantly, artifacts can hardly be observed. In the experimental results, significant artifacts can be observed in the standard limited view reconstruction, as shown in Fig. 7(d). Besides the undersampling of the wavefield, the noise as well as a wide range of the uncertainties in the experiment can also corrupt the measured data.[17] Reasonable estimation of the overall shape of this defect can still be achieved. The artifacts are significantly reduced by the regularization method, as shown in Fig. 7(e).

Figs. 8(a) and 8(b) show the cross-sections of the defect at the deepest depths along the horizontal direction in Fig. 7. The reconstructions using the data from the FE model and experiment slightly underestimate the depths of the defect by around 0.1 mm and 0.3 mm, respectively, as shown in Figs. 8(a) and 8(b). It is clear that by using regularization method a slightly better estimation of the defect profile and a reduction in artifacts can be achieved. In Fig. 8(b), the profiles of the defect, by using the experimental data, show slightly narrower than the true value, which are due to the limited accuracy of the standard limited view reconstruction and the choice of the thresholding level. It is worth mentioning that the overall level of artifacts shown in reconstructions of the irregularly shaped defect is relatively low, due to the relatively large range of viewing angles and small sampling spacing used in the measurement.[28]

B. Two defects

To demonstrate the suitability of this algorithm for multiple defects, two flat-bottom defects with relatively large

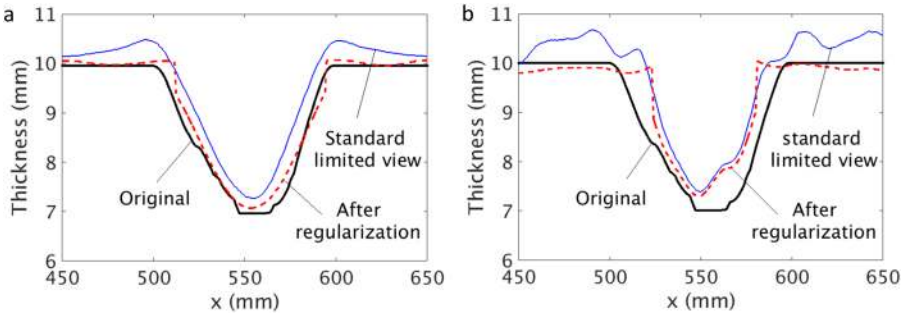

FIG. 8. Cross-sections of standard limited view FWI and regularized reconstructions of an irregularly shaped defect along the horizontal direction in the FE model (a) and the experiment (b).

difference in the depth are considered in the second model. This modeling is also carried out with a pair of parallel linear transducer arrays. The array consists 17 transducers with the separation distance of 40 mm, as shown in Fig. 9(a). The larger defect has the surface diameter of 60 mm (≃1.8 wavelengths at 60 kHz) and the bottom diameter of 44 mm (≃1.32 wavelengths at 60 kHz), with the deepest depth of 5 mm. The shallower one has the surface diameter and the bottom diameter of 42 mm (≃1.3 wavelengths at 60 kHz) and 34 mm (≃1 wavelength at 60 kHz), respectively, with 20% depth of the thickness of the plate. In this model, the choice of the frequencies and the number of iterations are the same as in the

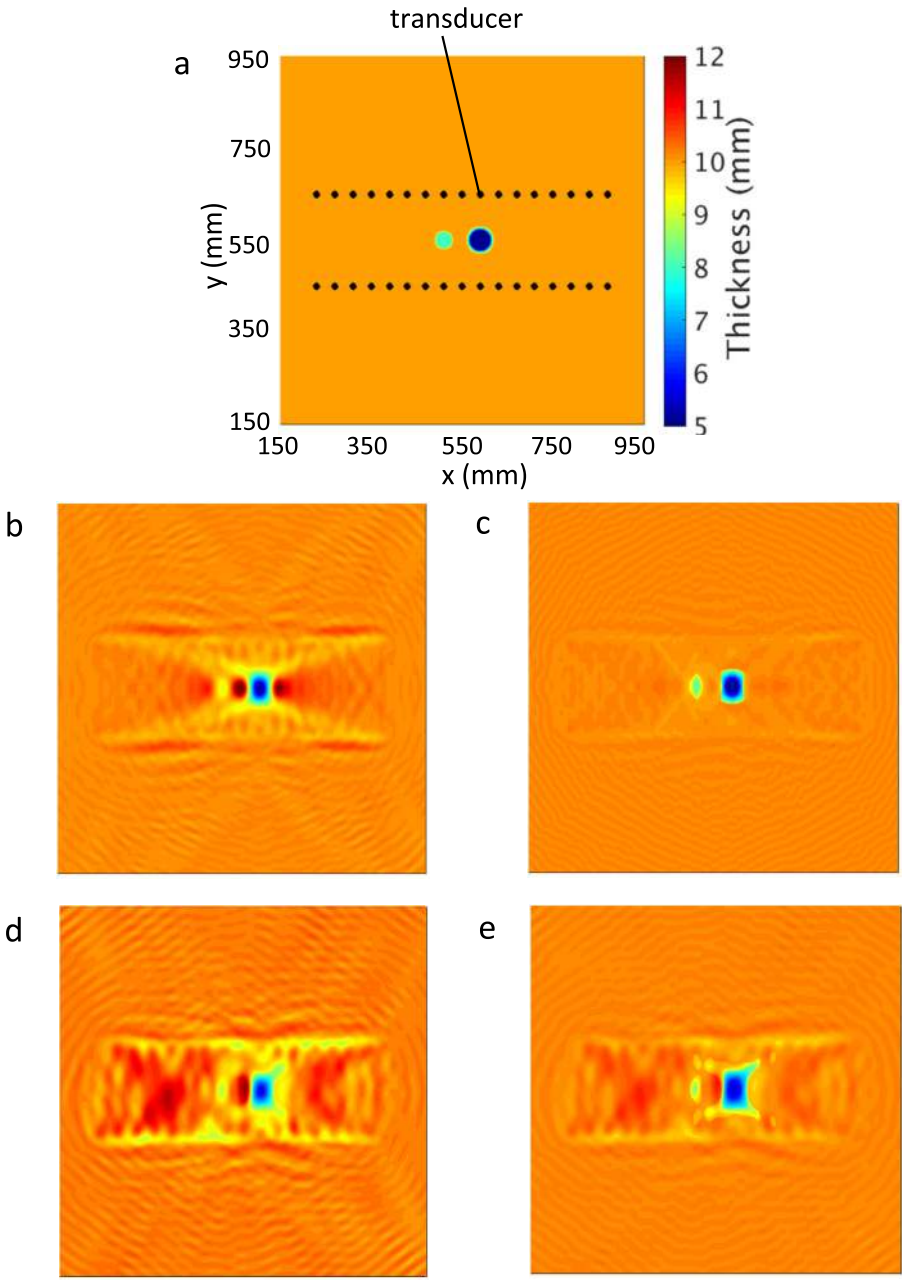

FIG. 9. Reconstructions with two flat-bottom defects by a pair of parallel linear transducer arrays. Original model (a), the standard limited view reconstruction (b), and the regularized reconstruction (c) based on the FE model; the standard limited view reconstruction (d), and the regularized reconstruction (e) based on the experiment. (b)–(e) follow the same color bar and scale in the axes as in (a).

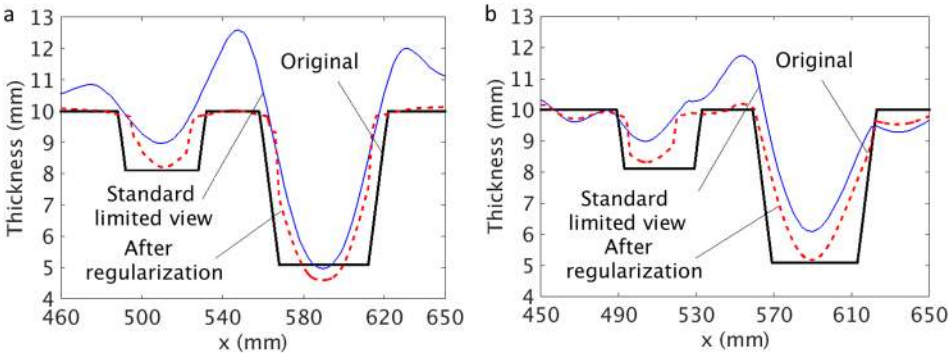

FIG. 10. Cross-sections of standard limited view FWI and regularized reconstructions of two flat-bottom defects along the horizontal direction in the FE model (a) and the experiment (b).

previous example. In the regularization, the starting level of threshold, slightly below the peak value of the shallower defect, is used to verify the capability of the regularization to distinguish shallower defect and the artifacts. It means that the starting model after the first regularization only contains the information of the larger defect without any information of the shallow defect. In this case, the whole process took about 2 h to obtain the improved reconstruction.

Figs. 9(b) and 9(d) show the standard limited view reconstruction based on the FE simulation and the experiment. It can be seen that, although the larger defects can be reasonably reconstructed, the smaller defects are almost shadowed by the artifacts. Significant improvement can be achieved by several iterations of regularization, as presented in Figs. 9(c) and 9(e). Both defects are clearly reconstructed, with the peak values captured initially and the low contrast features obtained by gradually increasing the threshold level. However, the diameter of the shallower defects seem to be smaller than the original defect size due to the reasons explained previously. There are obvious artifacts in the reconstruction obtained from the experiment and the main reasons were the undersampling of the wavefield and the noise.

Figs. 10(a) and 10(b) present cross-sectional reconstructions across the center of the defects along the horizontal direction. In Figs. 10(a) and 10(b), the larger defects can be accurately reconstructed in both standard limited view and regularized reconstructions from the FE simulation and the experiment, respectively. The regularized reconstructions of the shallower ones significantly improve the depth estimations compared to the standard limited view reconstructions, despite the sizes are smaller than the original one. Very few artifacts are visible in the regularized reconstructions, which are closer to the true values.

V. DISCUSSIONS

In Section IV, the work has focused on different types of defects with a relatively large range of angles. It enables a general analysis of the performance of the regularization to be identified. However, in reality, only a limited area is often allowed to place transducers, which significantly limits the range of viewing angles. In this section, a single flat-bottom defect was used to evaluate the influence of different array lengths with the data obtained from FE simulations and demonstrate the effectiveness of regularization. The surface and bottom diameters of the defect is 60 mm and 44 mm and its thickness reduction is 50%, as shown in Fig. 11(a). The varying ratio of the array length L to the fixed distance $D = 200$ mm between two arrays and the fixed sampling interval of 40 mm are considered. Figs. 11(b), 11(d), 11(f), 11(h) and 11(j) show the standard limited view reconstructions using a pair of linear arrays on each side of the defect, and Figs. 11(c), 11(e), 11(g), 11(i), and 11(k) show FWI with the adaptive thresholding regularization method.

It can be observed from Fig. 11(b) that when the ratio L/D is 4, good reconstruction of the defect can be obtained by using the standard limit view method with noticeable artifacts. Similar result can be achieved when the ratio L/D is equal to 3.2, as shown in Fig. 11(d). As the array reduces in length, the artifacts around the defect gradually expand. More clear distortions of the shape of the defect and underestimations in the peak contrasts can be observed in Figs. 11(f), 11(h) and 11(j). For this defect, the ratio L/D needs to be larger than 3.2 in order to obtain satisfactory results. Compared with the standard limited view results, the reconstructions after regularization can achieve improved images, with much fewer artifacts and better estimations of the contrast of defects. The improvement is still visible in the regularized image even when the ratio is very small, as shown in Fig. 11(k).

The critical information in the reconstruction of thickness maps is the maximum depth of the defect. Therefore, it is necessary to calculate the maximum depth error, which is defined as the difference between reconstruction depth and true depth divided by the nominal plate thickness.[17] Fig. 12 shows the maximum depth errors of FWI with and without regularization with respect to the ratio L/D. It is clear that the maximum depth errors are slightly reduced due to the additional information obtained from the regularization method. As the length of array increases, the viewing angles become larger, thus, reducing the reconstruction errors. The difference in the maximum depth errors of FWI with and without regularization extracted from Fig. 12 is listed in Table I. It is worth mentioning that the similar improvement trend can also be observed in the cases of irregularly shaped defect and two flat-bottom defects when applying the regularization approach.

VI. CONCLUSIONS

This paper has introduced the regularization technique to predict the missing components in the FWI algorithm with limited view configuration. The regularization is carried out by using an adaptive thresholding approach to the limited

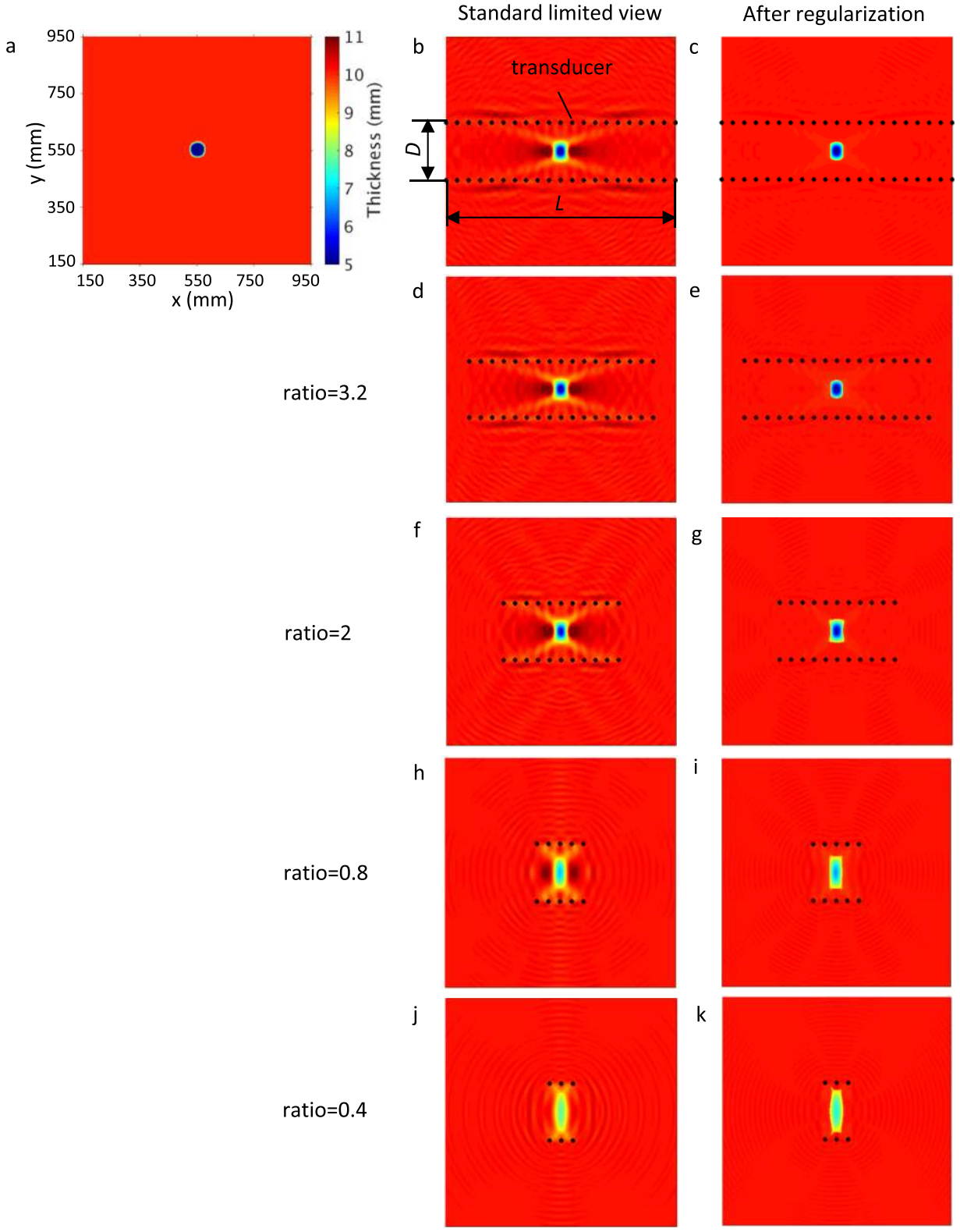

FIG. 11. Limited view reconstructions of a flat-bottom defect based on the FE model at 60 kHz. The first column shows the original model with defect depth of 5 mm and the surface diameter of 60 mm (a), the second column, that is, (b), (d), (f), (h), and (j) present the standard limited view reconstructions with FWI and the third column, that is, (c), (e), (g), (i), and (k) show FWI with regularization. In (b) and (c), the ratio L/D is 4; (d) and (e) reduce the ratio to 3.2, and (f) and (g) show ratio of 2. In (h) and (i), ratio is equal to 0.8 and (j) and (k) reduce that to 0.4. (b)–(k) follow the same color bar and scale in the axes as in (a).

view reconstruction. The performance of FWI algorithm with regularization to solve an irregular defect and two defects was demonstrated by using simulations as well as experiments. The results showed that the image quality is improved by combining the extra information through the regularization with measured data from the limit view configuration. When testing the regularization approach with limited view elastic data via the variation in the array length, similar improvement

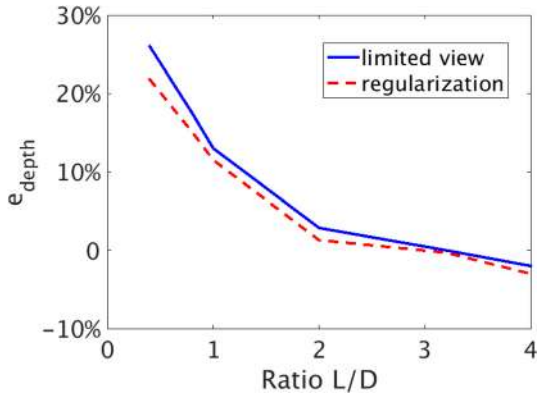

FIG. 12. The relationship between the ratio L/D and the maximum depth error e_{depth} with a single flat-bottom defect.

TABLE I. Comparison of the maximum depth errors (e_{depth}) between the reconstruction with and without regularization.

Methods \ ratio L/D	0.4	0.8	2	3.2	4
Standard limited view	26%	17.5%	2.9%	0%	−2%
Limited view with regularization	21.8%	15.1%	1.3%	−0.3%	−3%

can be achieved. This limited view configuration is very useful for pipes which can be assessed by two arrays on either side of the defect region. The reconstruction of the remaining wall thickness in pipes can be investigated by using this regularization technique in the future work.

ACKNOWLEDGMENTS

The work was funded in part under the Energy Innovation Research Programme (EIRP, Award No. NRF2014EWT-EIRP003-010), administrated by the Energy Market Authority (EMA). The EIRP is a competitive grant call initiative driven by the Energy Innovation Programme Office, and funded by the National Research Foundation (NRF). The authors are grateful to Dr. Peter Huthwaite for useful discussions.

[1]P. Belanger and P. Cawley, NDT E Int. **42**, 113 (2009).
[2]P. Huthwaite and F. Simonetti, Wave Motion **50**, 979 (2013).
[3]P. B. Nagy, F. Simonetti, and G. Instanes, Ultrasonics **54**, 1832 (2014).
[4]M. Davison, SIAM J. Appl. Math. **43**, 428 (1983).
[5]P. Huthwaite, A. A. Zwiebel, and F. Simonetti, IEEE Trans. Ultrason. Ferroelectr. Freq. Control **60**, 603 (2013).
[6]A. Andersen, IEEE Trans. Med. Imag. **8**, 50 (1989).
[7]A. Devaney, IEEE Trans. Geosci. Remote Sens. **22**, 3 (1984).
[8]N. Duric, P. Littrup, L. Poulo, and A. Babkin, Med. Phys. **34**, 773 (2007).
[9]M. C. Lawrence, M. A. Jaffer, and B. T. Sewell, Ultramicroscopy **31**, 285 (1989).
[10]M. Persson, D. Bone, and H. Elmqvist, Phys. Med. Biol. **46**, 853 (2001).
[11]S. LaRoque, E. Sidky, and X. Pan, J. Opt. Soc. Am. **25**, 1772 (2008).
[12]E. Sidky and X. Pan, Phys. Med. Biol. **53**, 4777 (2008).
[13]M. L. Reis and N. C. Roberty, Inverse Prob. **8**, 623 (1992).
[14]K. M. Hanson, *Image Recovery: Theory and Application* (Academic, New York, 1987), pp. 79–127.
[15]A. P. Dhawan, R. M. Rangayyan, and R. Gordon, Appl. Opt. **24**, 4013 (1985).
[16]A. Delaney and Y. Bresler, IEEE Trans. Image Process. **7**, 204 (1998).
[17]J. Rao, M. Ratassepp, and Z. Fan, IEEE Trans. Ultrason. Ferroelectr. Freq. Control **63**, 737 (2016).
[18]R. Seidl and E. Rank, Comput. Math. Appl. **72**, 879 (2016).
[19]P. Huthwaite, R. Ribichini, P. Cawley, and M. J. S. Lowe, IEEE Trans. Ultrason. Ferroelectr. Freq. Control **60**, 1165 (2013).
[20]M. Born and E. Wolf, *Principles of Optics* (Cambridge University Press, Cambridge, 1999).
[21]P. Huthwaite, "Quantitative imaging with mechanical waves," Ph.D. thesis (University of Imperial College, 2009).
[22]Y. Sung, W. Choi, C. Fang-Yen, and K. Badizadegan, Opt. Express **17**, 266 (2009).
[23]W. C. Chew and Y. M. Wang, IEEE Trans. Med. Imag. **9**, 218 (1990).
[24]P. Belanger, P. Cawley, and F. Simonetti, IEEE Trans. Ultrason. Ferroelectr. Freq. Control **57**, 1405 (2010).
[25]P. Rajagopal, M. Drozdz, E. Skelton, M. J. S. Lowe, and R. Craster, NDT E. Int. **51**, 30 (2012).
[26]M. Ratassepp, M. J. S. Lowe, P. Cawley, and A. Klauson, J. Acoust. Soc. Am. **124**, 2873 (2008).
[27]G. McMechan, J. Harris, and L. Anderson, Bull. Seismol. Soc. Am. **77**, 1945 (1987), see http://www.bssaonline.org/content/77/6/1945.short.
[28]A. Kak and M. Slaney, *Principles of Computerized Tomographic Reconstruction* (IEEE Press, New York, 1998).